Sedimentary Geology 480 (2025) 106853

Contents lists available at ScienceDirect

Sedimentary Geology

journal homepage: www.elsevier.com/locate/sedgeo

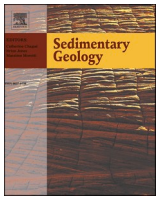

Trace element and OH content of quartz grains in the Amazon river: Potential application in provenance analysis

R. Stalder [a,*], D. Jaeger [a], S. Andò [b], E. Garzanti [b], C.M. Chiessi [c], A.O. Sawakuchi [d], T. Ludwig [e], M. Strasser [a]

[a] Universität Innsbruck, Innrain 52f, 6020 Innsbruck, Austria
[b] Laboratory for Provenance Studies, Department of Earth and Environmental Sciences, University of Milano-Bicocca, 20126 Milano, Italy
[c] School of Arts, Sciences and Humanities, University of São Paulo, Rua Arlindo Bettio 1000, CEP 03828-000 São Paulo, SP, Brazil
[d] Institute of Geosciences, University of São Paulo, Rua do Lago 562, CEP 05508-080 São Paulo, SP, Brazil
[e] Universität Heidelberg, Institut für Geowissenschaften, Im Neuenheimer Feld 234-236, 69120 Heidelberg, Germany

ARTICLE INFO

Editor: Dr. Massimo Moretti

ABSTRACT

Quartz grains in sediment carried by the Amazon River and five of its major tributaries were analyzed by FTIR-spectroscopy and secondary ion mass spectrometry to evaluate their potential for provenance analysis. Additionally, heavy mineral analysis was performed in the same samples to support sediment discrimination and provenance interpretation. Average defect water contents in quartz grains carried by branches with headwaters draining the Andes are higher (Solimões River 8.8 wt ppm, Madeira River 7.2 wt ppm) than in branches exclusively draining cratonic areas (Xingu River 6.5 wt ppm, Tapajós River 4.6 wt ppm, Negro River 4.7 wt ppm); values in one Amazon mainstem sample are intermediate with prevalence of the Andean signal (7.7 wt ppm). The average defect water content correlates to the fraction of grains that are defect-water rich (> 10 wt ppm), ranging from 30 to 40 % for the Solimões, Madeira, and Amazon Rivers down to 10–20 % for the Tapajós and Negro Rivers. The average molecular-water signal exhibits a much clearer contrast than the OH-defect signal. Grains from cratonic tributaries (Negro, Tapajós and Xingu rivers) exhibit significantly weaker molecular water signals than grains from Andean tributaries (Solimões and Madeira rivers); slightly weaker than the latter is the signal from grains in the Amazon mainstem, reflecting a mixture of Solimões and Negro rivers quartz in the Amazon mainstem sample.

In contrast, trace-element concentrations widely overlap among samples, preventing any robust discrimination about the sources of quartz grains. Trace metals show a fair correlation between Li and Al in all samples; a weak correlation between Al and Ti (indicative of igneous origin) was observed in Negro, Xingu and Amazon River sands, but not in Solimões, Madeira and Tapajós sands. Boron correlates with Li in Tapajós river and Amazon mainstem samples and with Al in Madeira and Tapajós samples.

Heavy-minerals are mostly amphibole, epidote, augitic clinopyroxene and hypersthene in Solimões River sands largely derived from the Andes, and andalusite, amphibole and epidote in Madeira River sands. Cratonic tributaries contribute durable tourmaline and zircon with andalusite (Negro River) or staurolite and topaz (Tapajós River).

The higher content of OH defects and molecular water in quartz grains derived from the Andes than in those from cratonic areas indicates that this property can provide useful complementary information to discriminate the source of quartz grains, one of the thorniest tasks in provenance analysis.

1. Introduction

Among rock-forming minerals, quartz does not only occur in sedimentary, plutonic, and metamorphic lithologies, but also shows the highest resistance to physical and chemical weathering. Consequently, it is the most abundant mineral in siliciclastic sediments. Depending on its formation conditions and thermal history, quartz can host significant amounts of trace metals and protons in its crystal lattice. These chemical

* Corresponding author.
E-mail address: roland.stalder@uibk.ac.at (R. Stalder).

https://doi.org/10.1016/j.sedgeo.2025.106853
Received 9 October 2024; Received in revised form 26 February 2025; Accepted 28 February 2025
Available online 1 March 2025

impurities are maintained throughout the sedimentary cycle and mostly preserve information on the initial crystallization conditions. Because metal impurities are immobile in the quartz crystal lattice, they have been used as a tool for provenance analysis (Ackerson et al., 2015). Protons, on the other hand, form OH-defects by coupled substitutions with metal cations that may be preserved over geological timescales (Stalder, 2014), but can be partly or completely reset at temperatures above 300–400 °C (Stalder et al., 2017). Therefore, OH-defects in quartz either serve as an archive for initial crystallization conditions (if OH-defects are still present) or indicate metamorphic overprint (if OH-defects are mostly annealed). In this way, a rough distinction between (young) igneous and (older) metamorphic sources is possible because pristine igneous quartz generally exhibits comparably high OH-defect concentrations, and metamorphic quartz is generally OH defect-poor (Stalder, 2021). OH-defect contents (henceforward called "defect water") have been successfully used to characterize and discriminate quartz grains from natural sources (Stalder et al., 2017, 2019; Jaeger et al., 2019; Potrafke et al., 2020). Using defect water contents in quartz has an interesting potential in provenance analysis for several reasons: (i) quartz represents the majority – commonly a very large majority – of sand grains, and yet no robust method has been devised to conclusively determine quartz provenance so far; (ii) quartz with different defect water contents has virtually the same density and thus behaves identically during erosion, transport and deposition, in contrast to heavy minerals that are markedly concentrated in specific size classes in the fine tail of the size distribution (Garzanti et al., 2009); and (iii) the durability difference under physical or chemical attack between quartz with low and high defect water content is expected to be much smaller than among different minerals.

In this study, defect water, molecular water, and trace metal contents from six sediment samples from the main rivers of the Amazon drainage basin were determined to evaluate their potential for provenance analysis. The samples were collected in the two main tributaries sourced in the Andes (Solimões and Madeira rivers), in the three main cratonic tributaries draining the Guiana and Central Brazilian shields and their sedimentary cover (Negro, Tapajós, and Xingu rivers), and finally in the Amazon mainstem close to the mouth (Fig. 1). Quartz grains were analyzed by Fourier-transform infrared-spectroscopy (henceforward FTIR) and secondary-ion-mass spectrometry (henceforward SIMS). In contrast to other provenance approaches that used Sr-Nd-isotopes (Allègre et al., 1996; Roddaz et al., 2005; Viers et al., 2008; Höppner et al., 2018), zircon ages (Louterbach et al., 2017), heavy minerals (Vital et al., 1999; Nascimento Jr. et al., 2015), or palynological results (Hoorn et al., 2017; Akabane et al., 2020), this study is based on quartz, the major component of the sediment load. In contrast to some previous studies based on quartz, where a distinction based on grain morphology was made among transporting *media* (e.g., glacier versus river; Rimington et al., 2000), we focus here on provenance with the aim to detect significant differences between orogenic (Andean) and cratonic (Guiana and Brazilian shields) origins. As a well-established provenance tools, heavy-mineral analysis and sand petrography were performed for comparison on the same samples and on three additional Amazon mainstem samples where quartz grains were too small to obtain valuable IR spectra.

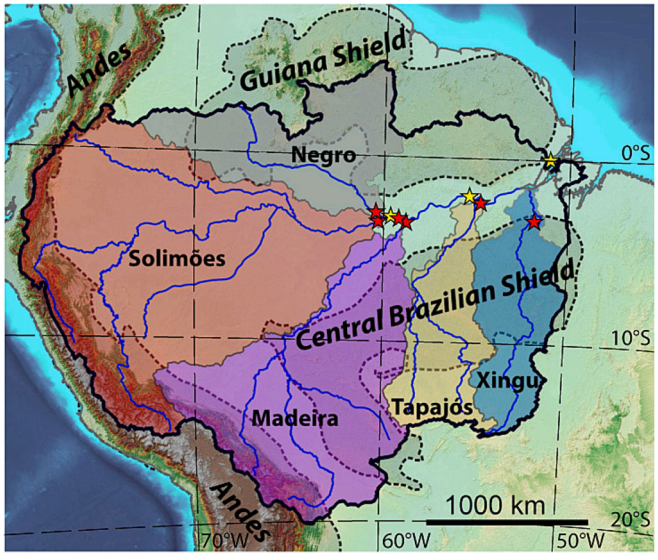

Fig. 1. Map of the Amazon river drainage basin (thick black line) showing the most important tributaries (color shading) and sample localities (yellow and red stars). Some samples were only analyzed for heavy minerals (yellow symbols), while some samples were analyzed for both quartz and heavy minerals (red symbols). Main geological units such as the Andes, the Guiana shield and the Brazilian shield are schematically depicted by dashed black lines. Latitudes and longitudes are shown as broken lines for orientation. For exact location of each sampling site see Table 1.

2. Geological background

The Amazon sedimentary system, largely fed from Andean orogenic sources, encompasses a huge west-to-east equatorial transcontinental drainage from the Andes to the Atlantic abyssal plain, feeding the third-largest active turbidite system on Earth. The modern drainage with huge delivery of terrigenous sediment to the ocean was presumably established in the late Miocene (e.g., Dobson et al., 2001; Figueiredo et al., 2009, 2010; Hoorn et al., 2017), due to surface processes related to the uplift of the central and northern Andes (e.g., Gregory-Wodzicki, 2000; Garzione et al., 2008), along with the flexural isostasy of the lithosphere (e.g., Shephard et al., 2010; Sacek, 2014). Estimates of transported sediment suggest an overwhelming dominance of Andean over cratonic material in the modern drainage system (e.g., Gibbs, 1967; Allègre et al., 1996; Dobson et al., 2001; Filizola and Guyot, 2009), even though the Andean cordillera only accounts for 12 % of the Amazon catchment area. Transport of Andean sediment through the Amazon basin as far as the Atlantic passive continental margin and beyond is documented by independent provenance studies (e.g., Rimington et al., 2000; Figueiredo et al., 2009, 2010; Gorini et al., 2014; Horton et al., 2015; Hoorn et al., 2017; Höppner et al., 2018; Sawakuchi et al., 2018). The Andean and cratonic affinities of the studied sediment samples were confirmed by a previous study using quartz optically stimulated luminescence (OSL) and elemental geochemistry (Sawakuchi et al., 2018). The Tapajós and Xingu tributaries drain the central Brazilian shield and both have strong seasonal variations in discharge (Latrubesse et al., 2005). The peak discharge of the Amazon mainstem exhibits a two months lag compared to that of the Tapajós and Xingu rivers, which causes strong backwater effects that prevent most of tributary suspended sediment from entering the Amazon mainstem (Fricke et al., 2017). Primary Andean sources of quartz include an important contribution of Phanerozoic igneous rocks while the primary Cratonic sources of quartz are mainly represented by Precambrian metamorphic rocks exposed in the shield areas (Gómez et al., 2019). It is also highlighted that both the Andean and Cratonic areas drained by the tributaries of the Amazon River have sedimentary rocks representing recycling of primary quartz sources (Milani and Zalán, 1999; Jaillard et al., 2000). Despite the Solimões and Madeira Rivers having Cratonic tributaries, Andean sources dominate their sand supply (Sawakuchi et al., 2018). Thus, as outlined in the introduction, dominant delivery of quartz from either of the two settings (Andean or shield) should therefore be distinguishable.

3. Samples and methods

Nine sediment samples collected during a previous sampling campaign (Sawakuchi et al., 2018) were chosen as test material for our new approach. These samples represent the five most important

tributaries of the Amazon River (i.e., Negro, Solimões, Madeira, Tapajós and Xingu Rivers) as well as four different localities in the mainstem of the Amazon River. Sample localities are summarized in Table 1 and graphically presented in Fig. 1. Sandy sediments were retrieved from the riverbed using a grab sampler. Detailed information on sampling surveys and sites can be found in Sawakuchi et al. (2018). Samples were submitted to wet sieving, and the quartz percentage was determined according to Garzanti (2019). Quartz grains from the size class 250–500 μm were manually prepared as grain mounts with thicknesses between 40 μm and 225 μm (140 μm on average). The thickness of each grain mount was measured with a mechanical micrometer and later corrected for each grain using the IR absorption of the lattice overtones (Stalder et al., 2017). Another set of grains from the same batch were randomly selected for trace-element analyses by SIMS. Based on the required minimum grain size for the FTIR analysis of quartz, only six of the samples were suitable for quartz analyses. Heavy-mineral analyses were performed for all samples.

3.1. FTIR spectroscopy

Polarised infrared absorption spectra were recorded at room temperature in transmission mode with a Bruker Vertex 70 FTIR spectrometer equipped with a silicon carbide (SiC) globar and a KBr beam splitter, which was coupled to a Hyperion 3000 microscope equipped with a nitrogen-cooled MCT-detector and a ZnSe wire grid polarizer (Stalder and Neuser, 2013; Stalder, 2014). 32–500 scans of each spectrum were acquired in the 550–7000 cm^{-1} range with a spectral resolution of 2 cm^{-1}. Typically, 42–64 quartz grains of each sample were analyzed by FTIR-spectroscopy.

Concerning data reduction, a new protocol was developed. Instead of two polarised measurements on oriented grains (Stalder and Konzett, 2012), polarised spectra were recorded from a grain mount with randomly oriented quartz grains. This simplification was possible because the boron-related OH-defects (BOH defects) were nearly absent in the analyzed grains. The BOH-dipole is the only one that has significant contributions in two crystallographic directions; all other OH-related absorption bands are oriented parallel to the refractive index n_o, which is exposed in any section of a quartz grain. Consequently, each grain was measured both parallel to n_ω and perpendicular to it. In the first spectrum, the maximum absorption of the OH-defect signal and (isotropic) molecular water signal (from fluid or melt inclusions) is displayed; the second spectrum shows the (isotropic) molecular-water signal and a reduced OH-defect signal (depending on the section angle through the crystal). From the silica overtones (well-known from previous studies for sections parallel to n_o and parallel to n_e; e.g. Stalder et al., 2017), the orientation (deviation from the sections parallel to n_e) can be determined and the spectrum for $E||n_e$ can thus be calculated. The further procedure for the background correction is described in Stalder and Konzett (2012). The calibration of Libowitzky and Rossman (1997) was used to calculate the defect-water content.

In addition to the OH-defect water, the molecular water signal (originating from fluid and hydrous melt inclusions) and the contribution of OH from hydrous mineral inclusions (particularly mica) was determined by adding the two recorded polarised spectra (equivalent to one unpolarised spectrum on each grain).

3.2. Secondary ion mass spectrometry (SIMS)

SIMS measurements were conducted on 21–23 quartz grains from each sediment sample. Concentrations of Li, B, Al, K, Ti, and Ge were measured using a CAMECA ims3f ion microprobe at the Institute of Earth Sciences, Heidelberg University. Analyzed grains other than quartz or analyzed spots containing mineral or melt inclusions were identified by high K concentrations (not reported here) and sorted out. The analytical strategy and technical details are summarized in Potrafke et al. (2020).

Table 1
Sample details and heavy mineral analysis. Numbers are given in % of grains. Samples are arranged from West to East.

sample	sample #	original ID*	Milan HM ID	latitude	longitude	Qz (%)	n (HM)	ZTR	Epidote	Garnet	Staurolite	Al_2SiO_5	Amph	Cpx	Opx	others
Solimões	AM_04	NSM10t	S5978	3.0359 S	60.5414 W	64	202	0	29	5	0	3	20	23	19	1
Negro	AM_03	MAO06b	S5977	3.3188 S	60.0798 W	99	97	51	1	0	4	41	0	0	0	3
Amazon	AM_09	NSM32g	S5979	3.1456 S	59.3249 W	54	200	2	20	3	1	1	39	19	13	5
Amazon	AM_06	MAO21d	S5980	3.2377 S	59.0301 W	n.a.	203	0	36	1	0	7	38	10	6	1
Madeira	AM_05	MAO32	S5981	3.3474 S	58.6892 W	65	203	3	31	3	0	1	25	20	13	3
Amazon	AM_08	STM02a	S5982	1.9320 S	55.4941 W	62	200	5	23	4	0	1	35	15	11	9
Tapajós	AM_02	STM18	S5983	2.4707 S	54.9818 W	99	92	27	1	0	42	3	0	0	0	26
Xingu	AM_06	XNG21	S5984	3.2612 S	52.0766 W	97	41	15	17	7	5	5	37	10	0	5
Amazon	AM_07	715	S5985	0.0636 S	51.0876 W	67	201	2	20	3	0	12	27	17	13	3

* from Sawakuchi et al. (2018); HM = heavy mineral; ZTR = zircon - tourmaline - rutile; n.a. = not analyzed.

3.3. Heavy-mineral analysis

Heavy minerals were separated by centrifuging in Na-polytungstate (2.90 g/cm^3) from a split aliquot of the 15–500 μm grain size fraction obtained by wet sieving of nine samples, and subsequently recovered by partial freezing with liquid nitrogen (Andò, 2020). If enough material was available, ≥ 200 transparent heavy minerals were point-counted for each sample (Garzanti and Andò, 2019). If less material was available, all grains from the grain mount were counted.

Transparent heavy-mineral (tHM) assemblages are defined as the spectrum of terrigenous minerals with density > 2.90 g/cm^3 identifiable under a transmitted-light microscope. Opaque minerals, rock fragments, iron oxides, soil clasts, phyllosilicates, and carbonates were not considered as integral part of the tHM suite. According to tHM concentration (tHMC index of Garzanti and Andò, 2007, 2019), tHM suites are described as "poor" (HMC < 1), "moderately poor" (1 ≤ tHMC <2), "moderately rich" (2 ≤ tHMC <5) or "rich" (tHMC >5). All dubious grains were checked with Raman spectroscopy (Andò and Garzanti, 2014). The ZTR index (sum of zircon, tourmaline, and rutile over total tHM; Hubert, 1962) expresses the durability of the tHM suite through multiple sedimentary cycles (Garzanti, 2017). The Amphibole Color Index (ACI) varies from 0 in detritus from low-grade metamorphic rocks yielding exclusively blue-green amphibole to 100 in detritus from granulite-facies or volcanic rocks yielding exclusively brown amphibole and oxy-hornblende (Andò and Garzanti, 2014).

4. Results

Sand samples from Andean tributaries Solimões and Madeira and the Amazon mainstem have sharply different petrographic composition than those of the three cratonic tributaries Negro, Tapajós, and Xingu (Table 1). Andean and Amazon mainstem samples are feldspatho-litho-quartzose and contain <70 wt% quartz, whereas sands from the Negro, Tapajós and Xingu rivers are pure quartzose (> 95 wt% quartz), following the classification by Garzanti (2019).

4.1. Quartz

Average IR spectra from all samples are similar and dominated by the AlOH triplet (Fig. 2). LiOH and BOH absorption bands are generally much weaker, most pronounced in Solimões grains, less frequent in mainstem Amazon and Xingu grains, and still less in the other samples. If LiOH and BOH bands (at 3470 and 3595 cm^{-1}, respectively) are visible in the average spectra, then they are based on the contribution of very few individual grains that exhibit pronounced LiOH and BOH bands (Fig. 3). Average defect water contents (Table 2, Fig. 4) are higher in quartz grains carried by rivers draining the Andes (Solimões 8.8 wt ppm, Madeira 7.2wt ppm) than in rivers draining cratonic areas (Xingu 6.5 wt ppm, Tapajós 4.6 wt ppm, Negro 4.7 wt ppm), and intermediate in the Amazon mainstem (~7.7 wt ppm). The average defect water content correlates with the proportion of water-poor (< 10 wt ppm) grains, ranging from 60 to 70 % for Solimões, Madeira, and lower Amazon to 80–90 % for Tapajós and Negro (Fig. 5).

A very informative difference resulted to be a by-product of FTIR analysis not intended to be considered initially: the average molecular water signal characterized by a broad absorption band between roughly 3000 and 3700 cm^{-1} (Fig. 6). This signal is much weaker in quartz grains of the Xingu, Negro and Tapajós tributaries draining cratonic areas than in Solimões and Madeira samples with headwaters of largely Andean origin; only slightly weaker than the latter is the signal in quartz grains of the Amazon mainstem. The shoulder around 3620 cm^{-1}, clearest in Amazon and Negro samples, is inferred to be related to mica inclusions in individual grains (Fig. 6).

Trace-metal contents analyzed by SIMS show fair to moderate correlations between Li and Al in all samples (Fig. 7), $R^2 > 0.7$ for Solimões and Negro and R^2 of 0.35 for Madeira; no clear correlations (respectively: no correlations for Tapajós and Madeira) were observed for Al –

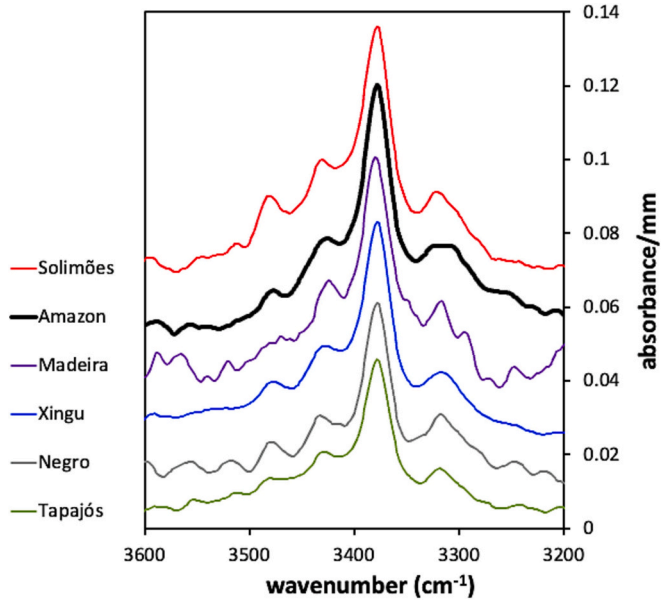

Fig. 2. Average IR absorption spectra for all six sediment samples normalized to 1 mm thickness. Spectra are based on two polarised measurements for 42–64 quartz grains (Table 2) in order to remove the isotropic part of the absorption signal (see text for further details).

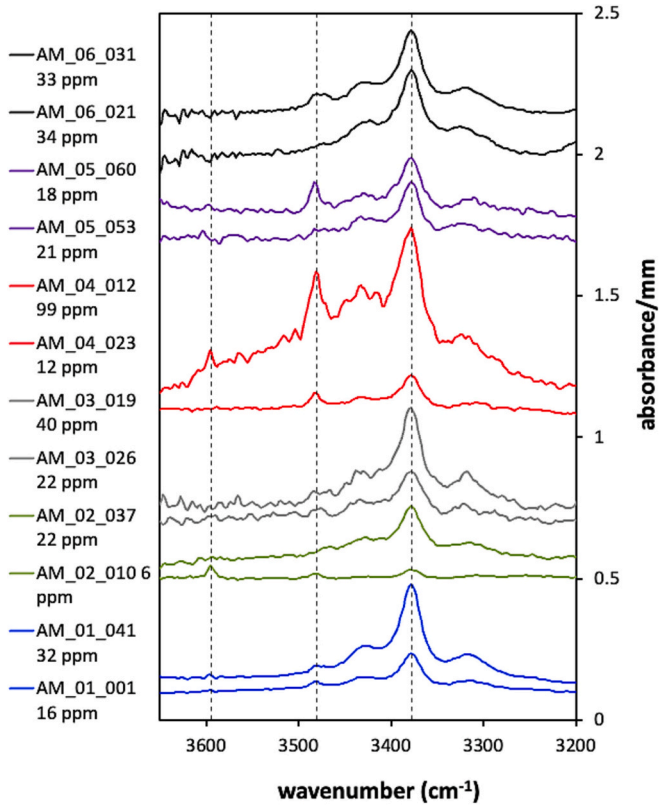

Fig. 3. Selected IR absorption spectra for individual quartz grain with high defect water content. Sample number and defect water contents are displayed in the legend. Vertical broken lines represent the specific absorption bands for BOH (3595 cm^{-1}), LiOH (3480 cm^{-1}) and AlOH (3378 cm^{-1}), respectively.

Table 2
Summary of SIMS and FTIR measurements (minimum, maximum, arithmetic mean, in wt. ppm) for Li, B, Al, Ti, and Ge for the Xingu, Tapajós, Negro, Solimões, Madeira, and lower Amazon river samples. b.d.l. = below detection limit.

sample	river	n (SIMS)		c (Li)	c (B)	c (Al)	c (Ti)	c (Ge)	n (FTIR)	c (OH)	c* (OH)
AM-01	Xingu	21	average	1.00	0.11	33.24	28.02	1.18	48	6.5	6.3
			min	b.d.l.	0.03	3.23	b.d.l.	0.22		b.d.l.	
			max	10.11	0.29	129.44	117.41	2.42		32.4	
AM-02	Tapajós	23	average	1.15	0.42	33.51	27.86	1.14	46	4.6	5.4
			min	b.d.l.	0.03	3.48	1.22	0.31		b.d.l.	
			max	10.27	2.35	119.17	209.50	2.71		22.0	
AM-03	Negro	22	average	0.75	0.19	27.84	26.96	1.15	64	4.7	4.7
			min	b.d.l.	b.d.l.	4.36	b.d.l.	0.37		b.d.l.	
			max	4.76	0.65	98.43	110.64	2.75		39.5	
AM-04	Solimões	21	average	2.29	0.32	87.60	22.08	1.67	42	8.8	11.1
			min	b.d.l.	0.02	3.94	b.d.l.	0.53		b.d.l.	
			max	26.93	0.93	1104.56	76.85	5.47		99.0	
AM-05	Madeira	23	average	0.48	0.25	32.55	22.11	1.30	50	7.2	6.7
			min	b.d.l.	0.02	2.69	0.10	0.27		b.d.l.	
			max	2.91	1.38	184.73	133.09	3.28		30.6	
AM-06	Amazon	21	average	0.84	1.35	43.11	33.64	1.28	43	7.7	9.0
			min	b.d.l.	0.04	2.07	0.25	0.24		b.d.l.	
			max	6.15	20.65	173.75	89.97	2.12		40.1	

c* (OH) is based on the averaged spectrum over all grains, while c (OH) is averaged over the water content of all individual grains.

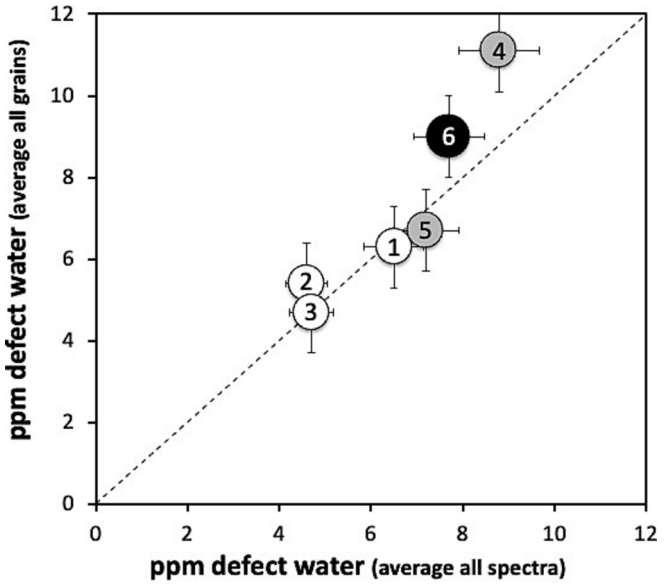

Fig. 4. Calculated average defect water content for quartz in all six sediment samples (Table 2). Two different strategies to calculate average water contents were followed: (1) the average defect water content was determined from the average absorption spectrum of all quartz grains, and (2) the average of the defect water content of all grains was calculated. This test was appropriate since many individual grains were around or below the detection limit.

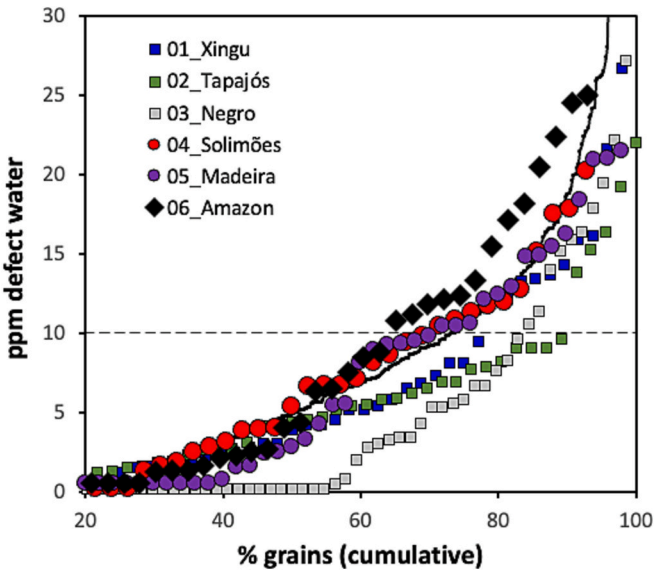

Fig. 5. Defect water distribution in all sediment samples. The black line represents the global average (Stalder, 2014). The broken line divides grains considered as water rich (>10 wt ppm) from average or water-poor grains. Water rich grains are more abundant in Amazon, Solimões and Madeira samples than in Xingu, Tapajós and Negro samples.

Ti and Li – Ti pairs. Weak correlations were observed for Li – B in Tapajós and Amazon samples and for B – Al in Tapajós and Madeira samples. No significant correlation between Al and Ti (indicative of origin from one igneous suite) was observed. Trace element contents show wide overlap among samples (e.g., Al/Ti is invariably ~1.5, and Li/B ~ 1), impeding discriminations among sediment samples (Fig. 7).

4.2. Heavy minerals

Andean and Amazon mainstem samples contain a moderately poor to moderately rich tHM suite consisting of amphibole, epidote-group minerals, clinopyroxene and hypersthene, with minor garnet (Fig. 8). Madeira sand contains andalusite with subordinate amphibole and epidote, and only a few pyroxenes (Limonta et al., 2015). Amphiboles include mainly blue-green hornblende and subordinately green-brown hornblende, oxy-hornblende and actinolite (ACI decreasing from ~30 to 15–20 downstream). Epidote-group minerals consist of epidote and clinozoisite with rare zoisite or allanite. Clinopyroxenes and orthopyroxenes are dominantly green augite and yellow-green hypersthene, respectively. Andalusite commonly shows oriented carbonaceous inclusions (chiastolite). Both pyralspite and grandite garnet in colourless, pink, and yellow-green varieties occur. Durable minerals include locally metamictic zircon, dravitic and schorlitic tourmaline, and rare rutile (ZTR 2 ± 2). Other minerals are represented by apatite, titanite, mainly fibrolitic sillimanite, and chloritoid. Grains of olivine, staurolite, kyanite, pumpellyite, vesuvianite, anatase, and brookite were also identified.

Negro, Tapajós and Xingu sands contain extremely poor tHM suites. Negro sand yielded andalusite (most grains showing carbonaceous inclusions), schorlitic and dravitic tourmaline, locally metamictic zircon, minor yellow and red rutile, kyanite with carbonaceous inclusions

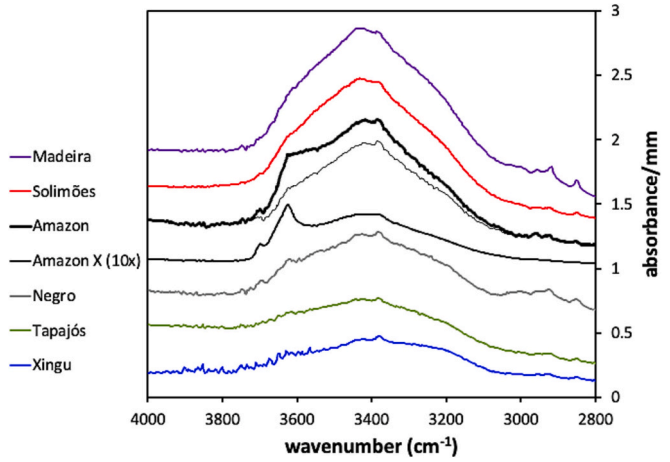

Fig. 6. Average IR spectra without subtraction of the isotropic signal, showing all OH contributions including defect water, fluid inclusions, melt inclusions, and mineral inclusions. The shoulder at 3620 cm^{-1} for the average spectrum of the Amazon sample is mostly caused by a single grain with abundant amounts of mica inclusions. If this grain (displayed as Amazon X diminished by a factor of 10!) is omitted from the average, the shoulder nearly disappears (thin line). The broad band for molecular water (between 3000 and 3700 cm^{-1}) of Amazon average spectrum reveals an absorbance in between the two Andean spectra (Solimões and Madeira) and the shield spectra (Xingu, Tapajós and Río Negro). Note the scale difference compared to Fig. 2, justifying the elimination procedure of the molecular signal in order to visualize the defect water signal.

(reticite), mainly prismatic sillimanite, staurolite, and rare apatite, clinozoisite, diaspore and an unidentified REE-bearing phosphate (ZTR 51). Tapajós sand yielded mainly staurolite with subordinate schorlitic and dravitic tourmaline, topaz, and minor inclusion-rich andalusite, zircon, red rutile, and rare corundum, monazite, anatase and clinozoisite (ZTR 27). Xingu sand yielded amphibole (blue-green hornblende and rare actinolite; ACI 0), epidote (pistacite with rare clinozoisite and Mn-epidote), and clinopyroxene (mostly green augite), with minor zircon, tourmaline, garnet, staurolite, and rare apatite, andalusite (viridine variety), prismatic sillimanite, and corundum (ZTR 15).

5. Discussion

Even if the observed difference in defect water in quartz among samples is subtle, a general trend from Solimões and Madeira (representing drainages dominated by Andean sediments, with minor cratonic material) to Xingu Tapajós, and Negro samples (representing cratonic material) is discernable. The higher defect water content in quartz grains from Solimões and Madeira with high contributions of quartz of younger crystallization age (in this case Andean) confirms previous observations that defects water in quartz is best retained in younger crystals (Stalder et al., 2017). The difference from sample to sample, however, is too small in our present case to calculate accurate mixture ratios. This result is unexpected, since in European case studies the defect-water content in quartz grains derived from the Precambrian shield (e.g., Scandinavian Proterozoic granites) and from Phanerozoic orogens (e.g., Central European Variscan massifs) differ by up to an order of magnitude (Stalder et al., 2017; Stalder, 2021). In modern sand from Baltic Sea beaches and large northern European river systems, the proportion of quartz grains transported by glaciers during the last glaciation increases northeastwards at the expense of Variscan sources with decreasing distance from the Scandinavian shield (Stalder et al., 2017, 2019). The discrepancy between the present case study and the previous studies in Northern Europe may be related to the different modal quartz content of the respective "young" source: the diverse igneous rocks of the Andean Cordillera have much lower quartz contents than the granitic rocks of the Variscan orogen in Europe, and thus their contribution to the quartz inventory of downstream sediments is much less visible.

The molecular water content (derived from fluid inclusions in quartz), even though never used for provenance analysis to the best of our knowledge so far, reveals a promising potential. The observed difference between Andean (higher contents) and cratonic sources (lower contents) fits well with previous findings: (1) Tapajós and Xingu sediments derived from the shield and sedimentary cover exhibit a higher OSL-sensitivity than sediments in the Solimões and Madeira rivers sourced in the Andes (Sawakuchi et al., 2018); and, (2) an anti-correlation between molecular water content and OSL (optical stimulated luminescence) sensitivity in quartz was observed (Sharma et al., 2017), leading to the conclusion that (3) Tapajós and Xingu samples have lower molecular water contents than Solimões and Madeira samples. The observed higher molecular water content in quartz grains derived from the Andes is plausible from theoretical considerations (similar as the tendency observed for OH-defects), because fluid inclusions in old rocks are more prone to go lost after long-term moderate thermal treatment. The molecular water content in quartz grains of the Amazon mainstem is intermediate between Andean and cratonic material, reflecting a mixture dominated by the Andean component. Specifically, the molecular water signature in quartz of mainstem sample AM_06 is just intermediate between that of Solimões and Negro samples, suggesting that the Negro river is a significant contributor of quartz to the Amazon sand flux. On the other hand, quartz percentage does not change significantly downstream of the Tapajós, and Xingu confluences, indicating that these rivers do not contribute much to the total sediment flux. This is in agreement with the backwater effect difficulting the transference of sediments from the Negro, Tapajós and Xingu to the Amazon mainstem (e.g., Fricke et al., 2017).

The shoulder at 3620 cm^{-1} observed in Amazon and Negro samples may not be significant, since it disappears when the contribution of the grain with the most intense signal from the average spectrum is removed (Fig. 6). Mica inclusions cause a very prominent signal at 3620 cm^{-1} (Stalder and Neuser, 2013) that may be visible in the average spectrum even if only a few quartz grains contain mica inclusion. The mica signal could represent a valuable tool to discriminate different quartz populations if present in a sufficient number of grains; however, in the present data set it was observed only in very few grains and could not be evaluated statistically.

Results from heavy-mineral analysis are broadly in agreement with previous studies (Vital et al., 1999; Nascimento Jr. et al., 2015) that showed a dominance of pyroxenes and hornblende in the detritus from Andean igneous rocks and higher input of metamorphic minerals such as andalusite from metamorphic rocks of the shield. The remarkable consistency of heavy-mineral spectra all along the Amazon mainstem as far as the delta indicates predominant supply by the Solimões headwaters, illustrated by typical Andean heavy minerals such as amphibole, epidote, and pyroxenes, in contrast to cratonic tributaries (Negro, Tapajós, Xingu) that contribute durable tourmaline and zircon (Vital et al., 1999). Because transparent-heavy-mineral concentration is an order of magnitude less in Negro sand than in Solimões sand, Negro river contribution is not apparent from the heavy-mineral suite, apart from a slight increase in andalusite downstream of its confluence. The increase in andalusite is more evident downstream of the Madeira confluence as far as the Amazon mouth, reflecting significant sediment supply from the Madeira river coupled with moderately poor heavy-mineral concentration in Madeira sand.

As far as the apparent discrepancy of the conclusions based on the analyses of quartz and the heavy mineral analysis is concerned, it is important to note that forward mixing calculations based on quartz and heavy minerals may not necessarily lead to the same results. In the case of the Amazon, Andean detritus has a much higher concentration of heavy minerals than detritus recycled from siliciclastic rocks of the Andean foothills, siliciclastic cover strata of the Brazilian and Guiana shields, and – to a lesser extent – quartz-rich sediments accumulated in the foreland basins and in the Amazonian lowlands. The Paleozoic and

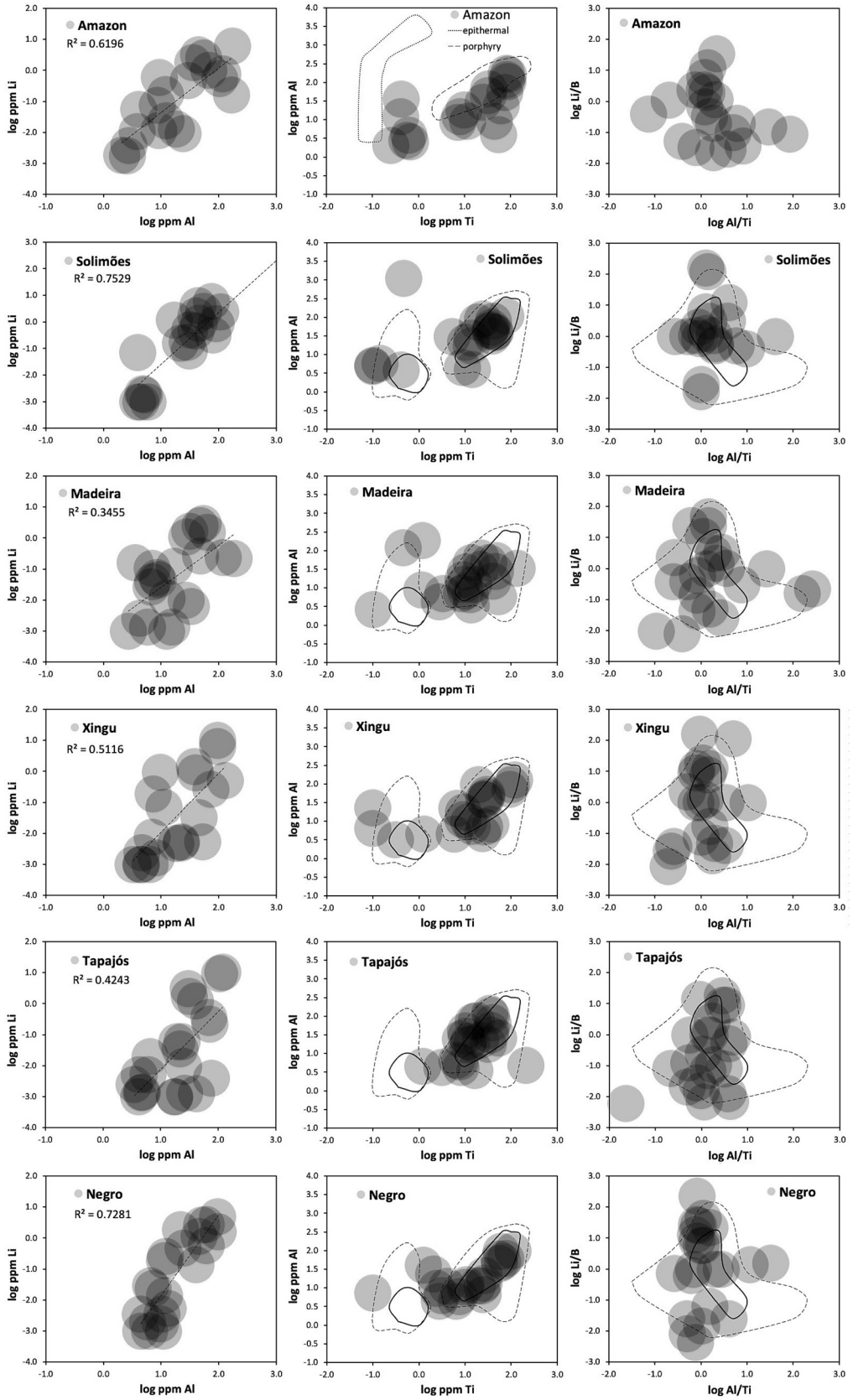

Fig. 7. Selected trace-element contents (in log μg/g) and trace element ratios of all sediment samples. Each analysis is shown as transparent data point and artificially enlarged in order to better illustrate the overlap of grain cluster. Analytical errors are far inside each data point. No diagnostic distinction among all sediment samples could be observed. Dotted and broken lines in the upper panel define the typical range for epithermal and porphyry quartz (Rusk, 2012; Götze et al., 2021). In all other panels bold solid lines and broken lines define the range of densest populations and range of appearance for the Amazon sample in the upper panel.

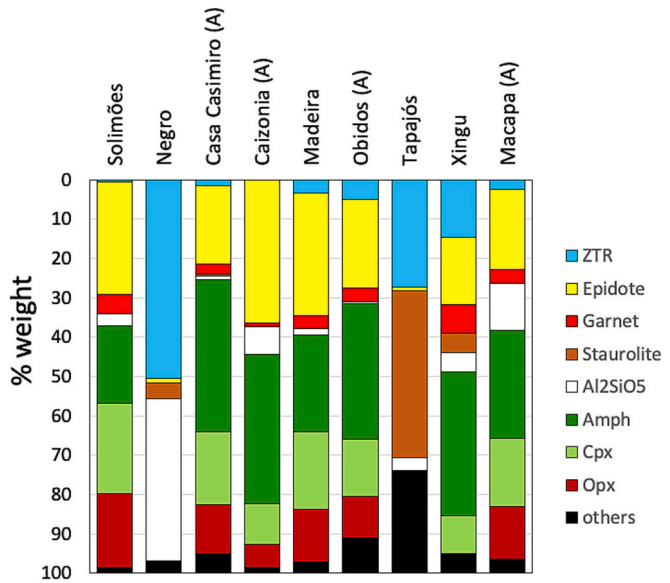

Fig. 8. Heavy-mineral spectra of studied sediment samples. For methodological details see Garzanti and Andò (2007, 2019), and Andò and Garzanti (2014).

Mesozoic sedimentary rocks overlaying the shield rocks in the watersheds of the Negro, Tapajós and Xingu have a Cratonic provenance signature, with heavy mineral assemblage dominated by metamorphic minerals (Mendes et al., 2019) while Cenozoic sediments accumulated in the lowlands of the Solimões watershed have Andean provenance (Horbe et al., 2019). Thus, the Andean and Cratonic provenance signals are maintained throughout sedimentary recycling, despite observed changes in mineral assemblages due to diagenesis and weathering.

6. Conclusions

The results of this study highlight both potential and limitations in the use of defect water, molecular water, and trace elements in quartz grains for provenance analysis on a continental scale. On the negative side, trace-element concentrations widely overlap among samples, preventing any robust discrimination among potential sources of quartz grains in this case study, which does not mean that trace elements may work as a valid discrimination tool in other cases. Another negative aspect is the increasing limitation of applicability of quartz if samples are too fine-grained. On a more positive side, average defect-water contents in quartz grains do show a difference between sand of rivers sourced in the Andes dominated by igneous and sedimentary Phanerozoic rocks and of tributaries draining cratonic Precambrian metamorphic rocks and their Paleozoic-Mesozoic covers (lower Negro, Tapajós, and Xingu rivers), reflecting a tendency to lose defect-water content over geological time. Based on defect water content, a dominant quartz supply from Andean branches with subordinate cratonic contribution is suggested in the Amazon mainstem sand samples. The average defect water content correlates with the percentage of grains that are rich in defect water (> 10 wt ppm), which is higher for Solimões, Madeira, and Amazon mainstem sands than for Tapajós and Negro sands. Molecular-water content, to the best of our knowledge never used for provenance analysis so far, is revealed as an unexpectedly promising tool for future provenance research. A strong diversity is revealed by the average molecular water signal, notably weaker in cratonic tributaries than in Andean headwater branches.

CRediT authorship contribution statement

R. Stalder: Writing – review & editing, Writing – original draft, Supervision, Resources, Project administration, Methodology, Investigation, Funding acquisition, Formal analysis, Data curation, Conceptualization. **D. Jaeger:** Formal analysis, Data curation. **S. Andò:** Writing – review & editing, Methodology, Investigation, Formal analysis, Data curation. **E. Garzanti:** Writing – review & editing, Methodology, Investigation, Formal analysis. **C.M. Chiessi:** Writing – review & editing, Methodology, Funding acquisition, Formal analysis. **A.O. Sawakuchi:** Writing – review & editing, Resources, Investigation, Funding acquisition. **T. Ludwig:** Methodology, Formal analysis, Data curation. **M. Strasser:** Writing – review & editing, Resources, Investigation, Funding acquisition, Conceptualization.

Declaration of competing interest

The authors declare the following financial interests/personal relationships which may be considered as potential competing interests: Roland Stalder reports financial support was provided by Austrian Science Fund. Christiano Chiessi reports financial support was provided by National Council for Scientific and Technological Development. Andre Sawakuchi reports financial support was provided by National Council for Scientific and Technological Development. If there are other authors, they declare that they have no known competing financial interests or personal relationships that could have appeared to influence the work reported in this paper.

Acknowledgements

This research project was funded by the Austrian Science Fund (FWF): P33038N. CMC acknowledges the financial support from FAPESP (grants 2018/15123-4 and 2019/24349-9), CNPq (grant 312458/2020-7) and CAPES-COFECUB (grants 8881.712022/2022-1 and 49558SM). AOS thanks the financial support by FAPESP (grant 2018/23899-2) and CNPq (grant 307179/2021-4). SA and EG acknowledge support from Project Dipartimenti di Eccellenza 2023–2027, Department of Earth and Environmental Sciences, University of Milano-Bicocca.

Appendix A. Supplementary data

Supplementary data to this article can be found online at https://doi.org/10.1016/j.sedgeo.2025.106853.

Data availability

Data will be made available on request.

References

Ackerson, M.R., Tailby, N.D., Watson, E.B., 2015. Trace elements in quartz shed light on sediment provenance. Geochemistry, Geophysics, Geosystems 16, 1894–1904. https://doi.org/10.1002/2015GC005896.

Akabane, T.K., Sawakuchi, A.O., Chiessi, C.M., Kern, A.K., Pinaya, J.L.D., Ceccantini, G. C.T., De Oliveira, P.E., 2020. Modern pollen signatures of Amazonian rivers and new insights for environmental reconstructions. Palaeogeography Palaeoclimatology Palaeoecology 554, 109802. https://doi.org/10.1016/j.palaeo.2020.109802.

Allègre, C.J., Dupré, B., Négrel, P., Gaillardet, J., 1996. Sr-Nd-Pb isotope systematics in Amazon and Congo River systems: Constraints about erosion processes. Chemical Geology 131, 93–112. https://doi.org/10.1016/0009-2541(96)00028-9.

Andò, S., 2020. Gravimetric separation of heavy minerals in sediments and rocks. Minerals 10, 273. https://doi.org/10.3390/min10030273.

Andò, S., Garzanti, E., 2014. Raman spectroscopy in heavy-mineral studies. Geol. Soc., London. Spec. Publ. 386, 395–412. https://doi.org/10.1144/sp386.2.

Dobson, D.M., Dickens, G.R., Rea, D.K., 2001. Terrigenous sediment on Ceara rise: a Cenozoic record of south American orogeny and erosion. Palaeogeography Palaeoclimatology Palaeoecology 165, 215–229. https://doi.org/10.1016/S0031-0182(00)00161-9.

Figueiredo, J., Hoorn, C., van der Ven, P., Soares, E., 2009. Late Miocene onset of the Amazon River and the Amazon deep-sea fan: evidence from the Foz do Amazonas Basin. Geology 37, 619–622. https://doi.org/10.1130/G25567A.1.

Figueiredo, J., Hoorn, C., van der Ven, P., Soares, E., 2010. Late Miocene onset of the Amazon River and the Amazon deep-sea fan: evidence from the Foz do Amazonas Basin. Reply to comment by Campbell K, Geology 38, 213. https://doi.org/10.1130/G31057Y.1.

Filizola, N., Guyot, J.L., 2009. Suspended sediment yields in the Amazon basin: an assessment using the Brazilian national data set. Hydrological Processes 23, 3207–3215. https://doi.org/10.1002/hyp.7394.
Fricke, A.T., Nittrouer, C.A., Ogston, A.S., Nowacki, D.J., Asp, N.E., Souza Filho, P.W.M., da Silva, M.S., Jalowska, A.M., 2017. River tributaries as sediment sinks: processes operating where the Tapajós and Xingu rivers meet the Amazon tidal river. Sedimentology 64, 1731–1753. https://doi.org/10.1111/sed.12372.
Garzanti, E., 2017. The maturity myth in sedimentology and provenance analysis. Journal of Sedimentary Research 87, 353–365. https://doi.org/10.2110/jsr.2017.17.
Garzanti, E., 2019. Petrographic classification of sand and sandstone. Earth-Science Reviews 192, 545–563. https://doi.org/10.1016/j.earscirev.2018.12.014.
Garzanti, E., Andò, S., 2007. Heavy mineral concentration in modern sands: Implications for provenance interpretation. In: Mange, M., Wright, D. (Eds.), Heavy Mineral in Use, Elsevier, Amsterdam, Developments in Sedimentology, vol. 58, pp. 517–545. https://doi.org/10.1016/S0070-4571(07)58020-9.
Garzanti, E., Andò, S., 2019. Heavy Minerals for Junior Woodchucks. Minerals 9, 148. https://doi.org/10.3390/min9030148.
Garzanti, E., Andò, S., Vezzoli, G., 2009. Grain-size dependence of sediment composition and environmental bias in provenance studies. Earth and Planetary Science Letters 277, 422–432. https://doi.org/10.1016/j.epsl.2008.11.007.
Garzione, C.N., Hoke, G.D., Libarkin, J.C., Withers, S., MacFadden, B., Eiler, J., Ghosh, P., Mulch, A., 2008. Rise of the Andes. Science 320, 1304–1307. https://doi.org/10.1126/science.1148615.
Gibbs, R.J., 1967. The geochemistry of the Amazon River System, part I: the factors that control the salinity and the composition and concentration of the suspended solids. Geological Society of America Bulletin 78, 1203–1232. https://doi.org/10.1130/0016-7606(1967)78[1203:TGOTAR]2.0.CO;2.
Gómez, J., Schobbenhaus, C., Montes, N.E. (compilers), 2019. Geological Map of South America 2018. Scale 1:5 000 000. Commission for the Geological Map of the World (CGMW), Colombian Geological Survey and Geological survey of Brazil. Paris.
Gorini, C., Haq, B.U., Reis, A.T., Silva, C.G., Cruz, A., Soares, E., Grangeon, D., 2014. Late Neogene sequence stratigraphic evolution of the Foz do Amazonas Basin, Brazil. Terra Nova 26, 179–185. https://doi.org/10.1111/ter.12083.
Götze, J., Pan, Y., Müller, A., 2021. Mineralogy and mineral chemistry of quartz: a review. Mineralogical Magazine 85, 639–664. https://doi.org/10.1180/mgm.2021.72.
Gregory-Wodzicki, K.M., 2000. Uplift history of the Central and Northern Andes: A review. GSA Bulletin 112, 1091–1105. https://doi.org/10.1130/0016-7606(2000)112<1091:Uhotca>2.0.Co;2.
Hoorn, C., Bogotá-A, G.R., Romero-Baez, M., Lammertsma, E.I., Flantua, S.G.A., Dantas, E.L., Dino, R., Carmo, D.A., Chemale, F., 2017. The Amazon at sea: onset and stages of the Amazon River from a marine record, with special reference to Neogene plant turnover in the drainage basin. Global and Planetary Change 153, 51–65. https://doi.org/10.1016/j.gloplacha.2017.02.005.
Höppner, N., Lucassen, F., Chiessi, C.M., Sawakuchi, A.O., Kasemann, S., 2018. Holocene provenance shift of suspended particulate matter in the Amazon River basin. Quaternary Science Reviews 190, 66–80. https://doi.org/10.1016/j.quascirev.2018.04.021.
Horbe, A.M.C., Roddaz, M., Gomes, L.B., Castro, R.T., Dantas, E.L., Carmo, D.A., 2019. Provenance of the Neogene sediments from the Solimões Formation (Solimões and Acre Basins), Brazil. Journal of South American Earth Sciences 93, 232–241. https://doi.org/10.1016/j.jsames.2019.05.004.
Horton, B.K., Anderson, V.J., Caballero, V., Saylor, J.E., Parra, M., Mora, A., 2015. Application of detrital zircon U-Pb geochronology to surface and subsurface correlations of provenance, paleodrainage, and tectonics of the Middle Magdalena Valley Basin of Colombia. Geosphere 11, 1790–1811. https://doi.org/10.1130/GES01251.1.
Hubert, J.F., 1962. A zircon–tourmaline–rutile maturity index and the interdependence of the composition of heavy minerals assemblages with the gross composition and texture of sandstones. Journal of Sedimentary Petrology 32, 440–450. https://doi.org/10.1306/74D70CE5-2B21-11D7-8648000102C1865D.
Jaeger, D., Stalder, R., Masago, H., Strasser, M., 2019. OH defects in quartz as provenance tool: Application to sediments from SW Japan. Sedimentary Geology 388, 66–80. https://doi.org/10.1016/j.sedgeo.2019.05.003.
Jaillard, E., Hérail, G., Monfret, T., Díaz-Martínez, E., Baby, P., Lavenu, A., Dumont, J.F., 2000. Tectonic evolution of the Andes of Ecuador, Peru, Bolivia and northernmost Chile. In: Cordani, U.G., Thomaz-Filho, A., Campos, D.A. (Eds.), Tectonic Evolution of South America, Acad. Bras. Cienc. Spec. Publ. 31st Int. Geol. Cong. (2000), pp. 41–95.
Latrubesse, E.M., Stevaux, J.C., Sinha, R., 2005. Tropical Rivers. Geomorphology 70, 187–206. https://doi.org/10.1016/j.geomorph.2005.02.005.
Libowitzky, E., Rossman, G.R., 1997. An IR calibration for water in minerals. American Mineralogist 82, 1111–1115. https://doi.org/10.2138/am-1997-11-1208.
Limonta, M., Garzanti, E., Resentini, A., Andò, S., Boni, M., Bechstädt, T., 2015. Multicyclic sediment transfer along and across convergent plate boundaries (Barbados, Lesser Antilles). Basin Research 27, 696–713. https://doi.org/10.1111/bre.12095.
Louterbach, M., Roddaz, M., Antoine, P.O., Marivaux, L., Adnet, S., Bailleul, J., Dantas, E., Santos, R.V., Chemale Jr., F., Baby, P., Sanchez, C., Calderon, Y., 2017. Provenance record of late Maastrichian-late Palaeocene Andean Mountain building in the Amazonian retroarc foreland basin (Madre de Dios basin, Peru). Terra Nova 30, 17–23. https://doi.org/10.1111/ter.12303.
Mendes, A.C., Silva, E.F., Fonseca, A.I.T., Nogueira, A.C.R., Silva, T.F., Nascimento, J.S. S., Igreja, H.F.E., 2019. Provenance of Upper Pennsylvanian siliciclastic-carbonate deposits from the Monte Alegre and Itaituba formations, North Brazil: an integrated study of sandstone petrography, heavy mineral analysis and garnet geochemistry. Geological Journal 55 (6), 4398–4414. https://doi.org/10.1002/gj.3676.
Milani, E.J., Zalán, P.V., 1999. An outline of the geology and petroleum systems of the Paleozoic interior basins of South America. Episodes 22 (3), 199–205. https://doi.org/10.18814/epiiugs/1999/v22i3/007.
Nascimento Jr., D.R., Sawakuchi, A.O., Guedes, C.C.F., Giannini, P.C.F., Grohmann, C.H., Ferreira, M.P., 2015. Provenance of sands from the confluence of the Amazon and Madeira rivers based on detrital heavy minerals and luminescence of quartz and feldspar. Sedimentary Geology 316, 1–12. https://doi.org/10.1016/j.sedgeo.2014.11.002.
Potrafke, A., Breiter, K., Ludwig, T., Neuser, R.D., Stalder, R., 2020. Variations of OH defects and chemical impurities in quartz within igneous bodies. Physics and Chemistry of Minerals 47, 24. https://doi.org/10.1007/s0026 9-020-01091-w.
Rimington, N., Cramp, A., Morton, A., 2000. Amazon Fan sands: implications for provenance. Marine and Petroleum Geology 17, 267–284. https://doi.org/10.1016/S0264-8172(98)00080-4.
Roddaz, M., Viers, J., Brusset, S., Baby, P., Hérail, G., 2005. Sediment provenances and drainage evolution of the Neogene Amazonian foreland basin. Earth and Planetary Science Letters 239, 57–78. https://doi.org/10.1016/j.epsl.2005.08.007.
Rusk, B., 2012. Cahodoluminescent Textures and Trace Elements in Hydrothermal Quartz. In: Götze, J., Möckel, R. (Eds.), Quartz: Deposits, Mineralogy and Analytics. Springer Geology, Heidelberg, New York, Dordrecht, London, pp. 307–330. https://doi.org/10.1007/978-3-642-22161-3_14.
Sacek, V., 2014. Drainage reversal of the Amazon River due to the coupling of surface and lithospheric processes. Earth and Planetary Science Letters 401, 301–312. https://doi.org/10.1016/j.epsl.2014.06.022.
Sawakuchi, A.O., Jain, M., Mineli, T.D., Nogueria, L., Bertassoli Jr., D.J., Häggi, C., Sawakuchi, H.O., Pupim, F.N., Grohmann, D.H., Chiessi, C.M., Zabel, M., Mulitza, S., Mazoca, C.E.M., Cunha, D.F., 2018. Luminescence of quartz and feldspar fingerprints provenance and correlates with source area denudation in the Amazon River basin. Earth and Planetary Science Letters 492, 152–162. https://doi.org/10.1016/j.epsl.2018.04.006.
Sharma, S.K., Chawla, S., Sastry, M.D., Gaonkar, M., Mane, S., Balaram, V., Singhvi, A.K., 2017. Understanding the reasons for variations in luminescence sensitivity of natural quartz using spectroscopic and chemical studies. Proceedings of the Indian National Science Academy 83, 645–653. https://doi.org/10.16943/PTINSA/2017/49024.
Shephard, G.E., Müller, R.D., Liu, L., Gurnis, M., 2010. Miocene drainage reversal of the Amazon River driven by plate-mantle interaction. Nature Geoscience 3, 870–875. https://doi.org/10.1038/ngeo1017.
Stalder, R., 2014. OH-defect content in detrital quartz grains as an archive for crystallization conditions. Sedimentary Geology 307, 1–6. https://doi.org/10.1016/j.sedgeo.2014.04.002.
Stalder, R., 2021. OH point defects in quartz – a review. European Journal of Mineralogy 33, 145–163. https://doi.org/10.5194/ejm-33-145-2021.
Stalder, R., Konzett, J., 2012. OH-defects in quartz in the system quartz – albite – water and granite – water between 5 and 25 kbar. Physics and Chemistry of Minerals 39, 817–827. https://doi.org/10.1007/s00269-012-0537-5.
Stalder, R., Neuser, R.D., 2013. OH-defects in detrital quartz grains: potential for application as tool for provenance analysis and overview over crustal averagse. Sedimentary Geology 294, 118–126. https://doi.org/10.1016/j.sedgeo.2013.05.013.
Stalder, R., Potrafke, A., Billström, K., Skogby, H., Meinhold, G., Gögele, C., Berberich, T., 2017. OH-defects in quartz as monitor for igneous, metamorphic and sedimentary processes. American Mineralogist 102, 1832–1842. https://doi.org/10.2138/am-2017-6107.
Stalder, R., von Eynatten, H., Costamoling, J., Potrafke, A., Dunkl, I., Meinhold, G., 2019. OH in detrital quartz grains as tool for provenance analysis: case studies on various settings from Cambrian to recent. Sedimentary Geology 389, 121–126. https://doi.org/10.1016/j.sedgeo.2019.06.001.
Viers, J., Roddaz, M., Filizola, N., Guyot, J.L., Sondag, F., Brunet, P., Zouiten, C., Boucayrand, C., Martin, F., Boaventura, G.R., 2008. Seasonal and provenance controls on the Nd-Sr isotopic compositions of the Amazon rivers suspended sediments and implications for Nd and Sr fluxes. Earth and Planetary Science Letters 274, 511–523. https://doi.org/10.1016/j.epsl.2008.08.011.
Vital, H., Stattegger, K., Garbe-Schönberg, C.D., 1999. Composition and trace-element geochemistry of detrital clay and heavy-mineral suites of the lowermost Amazon river: a provenance study. Journal of Sedimentary Research 69, 563–575. https://doi.org/10.2110/jsr.69.563.